POLITECNICO DI TORINO
Repository ISTITUZIONALE

Geometry-based surrogate modelling for peak stress assessment in flat and cross-curved bone plates subjected to transverse bending

Original
Geometry-based surrogate modelling for peak stress assessment in flat and cross-curved bone plates subjected to transverse bending / Bologna, F.A., Konopada, U., Carbonaro, D., Audenino, A., Terzini, M.. - In: RESULTS IN ENGINEERING. - ISSN 2590-1230. - ELETTRONICO. - 32:(2026). [10.1016/j.rineng.2026.111990]

Availability:
This version is available at: 11583/3015132 since: 2026-09-03T10:41:46Z

Publisher:
Elsevier

Published
DOI:10.1016/j.rineng.2026.111990

Terms of use:

This article is made available under terms and conditions as specified in the corresponding bibliographic description in the repository

Publisher copyright

(Article begins on next page)

19 November 2026

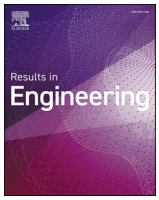
Results in Engineering 32 (2026) 111990



Contents lists available at ScienceDirect

Results in Engineering

journal homepage: www.sciencedirect.com/journal/results-in-engineering



Research paper

Geometry-based surrogate modelling for peak stress assessment in flat and cross-curved bone plates subjected to transverse bending

Federico Andrea Bologna [a,c,*], Ulyana Konopada [a,c], Dario Carbonaro [a,b,c], Alberto Audenino [a,c], Mara Terzini [a,c]

[a] Department of Mechanical and Aerospace Engineering, Politecnico di Torino, Turin, Italy
[b] Department of Mechanical, Energy and Management Engineering, University of Calabria, Rende, Italy
[c] Polito^{BIO}Med Lab, Politecnico di Torino, Turin, Italy

ARTICLE INFO

Keywords:
Bone plates
Cross-curved plates
Transverse bending
Stress concentration factor
ASTM F382-24

ABSTRACT

The increasing geometrical complexity of bone plates, driven by the adoption of anatomically precontoured designs to improve fit and biomechanical performance, requires efficient tools for structural evaluation to support implant design. Finite Element (FE) simulations provide accurate stress evaluations but remain computationally demanding when multiple design iterations are required. Moreover, existing analytical approaches for stress concentration factor (SCF) estimation are mainly limited to simplified geometries and do not account for the cross-curvature typical of commercial bone plates. This study develops a geometry-based computational framework for rapid SCF estimation in bone plates subjected to transverse bending under the pure bending condition representative of the ASTM F382-24 four-point bending test. FE simulations were combined with a Design of Experiments (DOE) approach to generate a dataset representative of commercial plate geometries, including thickness, width, hole diameter, and cross-curvature radius. Surrogate polynomial (SP) models were then developed to predict SCFs directly from plate geometry, enabling rapid estimation of peak bending stresses without repeated FE analyses. The developed models were validated on thirteen commercial bone plates excluded from the training dataset by comparing peak bending stresses obtained from SP-predicted SCFs and full FE simulations. The SP models showed strong predictive capability, with coefficients of determination up to $R^2 = 0.95$ and most stress prediction errors below 10%. Cross-curvature significantly affected SCF estimation, producing variations up to 18% compared with flat-plate assumptions. This framework provides a rapid computational tool for screening bone plate designs, enabling efficient mechanical assessment of anatomically contoured implants while reducing reliance on time-consuming FE simulations.

Notation

t	plate thickness
w	plate width
d	hole diameter
r	curvature radius (cross-curvature radius)
σ_{max}	maximum von Mises stress
σ_{nom}	nominal stress
SCF	stress concentration factor ($\sigma_{max}/\sigma_{nom}$)

Introduction

In orthopaedic surgery, bone plates are essential to ensure fracture stabilization and promote effective bone healing. Their design has evolved from simple, straight geometries to more anatomically shaped implants that conform to the bone's curvature, improving biomechanical compatibility and clinical outcomes [1]. These geometric adaptations are designed to improve implant-bone conformity and reduce implant prominence, which may enhance mechanical performance and minimize adverse interactions with surrounding soft tissues [2]. From a regulatory perspective, the mechanical performance of these devices is typically assessed through standardised experimental protocols, most commonly the four-point bending test defined by the ASTM F382 standard [3], which provides a reference framework for evaluating stiffness, strength, and fatigue behaviour of bone plates [4]. However, the increasing geometric complexity of bone plates, often featuring cross

* Corresponding author.
E-mail address: federico.bologna@polito.it (F.A. Bologna).

https://doi.org/10.1016/j.rineng.2026.111990
Received 4 May 2026; Received in revised form 25 June 2026; Accepted 13 July 2026
Available online 15 July 2026
2590-1230/© 2026 The Author(s). Published by Elsevier B.V. This is an open access article under the CC BY-NC-ND license (http://creativecommons.org/licenses/by-nc-nd/4.0/).

curvature, complicates the analytical estimation of stresses, which is particularly valuable in the early phases of device design.

Accurate stress assessment is indeed not only essential for ensuring long-term implant reliability and minimizing the risk of failure, but also for design optimization. Finite Element (FE) analysis has become a standard approach for evaluating stress distributions in such implants, especially when dealing with design features like holes [5–7] or notches [8]. Nonetheless, FE simulations often require high computational effort, limiting their practicality in iterative design or intraoperative planning [9].

In contrast, analytical methods offer faster estimations but usually simplify the problem by considering idealized, flat plates [10]. These models typically incorporate geometric discontinuities using Stress Concentration Factors (SCFs) derived from empirical studies over a limited range of values. However, they often neglect parameters such as the plate's cross curvature, which may influence the local stress distribution but has received limited attention in existing models.

Comprehensive investigations into stress concentrations around holes in infinite thin plates (See Appendix A, Eq. A1), idealized as two-dimensional bodies, under various loads have been documented by Pilkey [11] and Young and Budynas [12]. Additionally, it is widely acknowledged that the stress field in three dimensions, especially near a hole, is far more complex, and only a limited number of analytical solutions exist. Empirical formulas have been derived through fitting numerical results [13]. The classic Kirchhoff–Love plate theory, was usually applied to study stress around circular holes under bending. This theory is valid for thin plates, where the thickness (t) is much smaller than the hole diameter (d), but it neglects transverse shear deformation. More recently, She and Guo [14] validated empirical SCFs for isotropic plates with elliptical holes under tension, showing deviations from FE results within 1.5%. FE analysis has also been directly employed to compute SCFs. Bakhshandeh et al. [15] investigated a finite-width flat rectangular plate with a central circular hole under uniaxial tensile loading, including the influence of material orthotropy.

More recently, SCF quantification has also been investigated through data-driven and statistical approaches in structural engineering applications, where direct numerical evaluation may become computationally demanding [16–18]. These studies highlight the potential of surrogate-based approaches for efficiently capturing the relationship between geometric parameters, loading conditions, and stress concentration effects.

Despite these contributions, no SCF formulations are currently available for plates with holes under transverse bending in the common range of diameter-to-width ratios (d/w) greater than 0.3 (See Appendix A, Eq. A2), a range frequently found in commercial osteosynthesis implants. Additionally, no prior studies appear to have addressed the effect of cross curvature on SCF values. This study aims to fill this gap by developing a computational framework to determine accurate SCF values for flat and cross-curved plates under transverse bending. Through a Design of Experiments (DOE) approach, a wide parametric space was explored using FE simulations, and the resulting data were used to build a surrogate polynomial (SP) model for fast SCF prediction.

The aim of the work is to enable accurate assessment of peak bending stress in anatomically contoured bone plates without the need for full-scale FE analyses, thereby accelerating early-stage structural evaluations to support bone plate design and optimization.

Materials and methods

To implement the proposed computational framework, a structured pipeline was established starting from the extraction of geometric parameters from a representative sample of commercial bone plates (Fig. 1A). These parameters were used to define the design space for a full factorial DOE, implemented via parametric FE simulations. The resulting stress values were used to fit An SP model capable of approximating the SCF across varying geometries and curvatures (Fig. 1B). Separate SP models were developed and assessed for flat and cross-curved plates (Fig. 1C). Finally, the SP models were embedded into a MATLAB-based graphical user interface (GUI).

Dimension range extraction

A selection of thirteen bone plates was made to include various cross-sections (Fig. 2), with dimensions falling within the range of

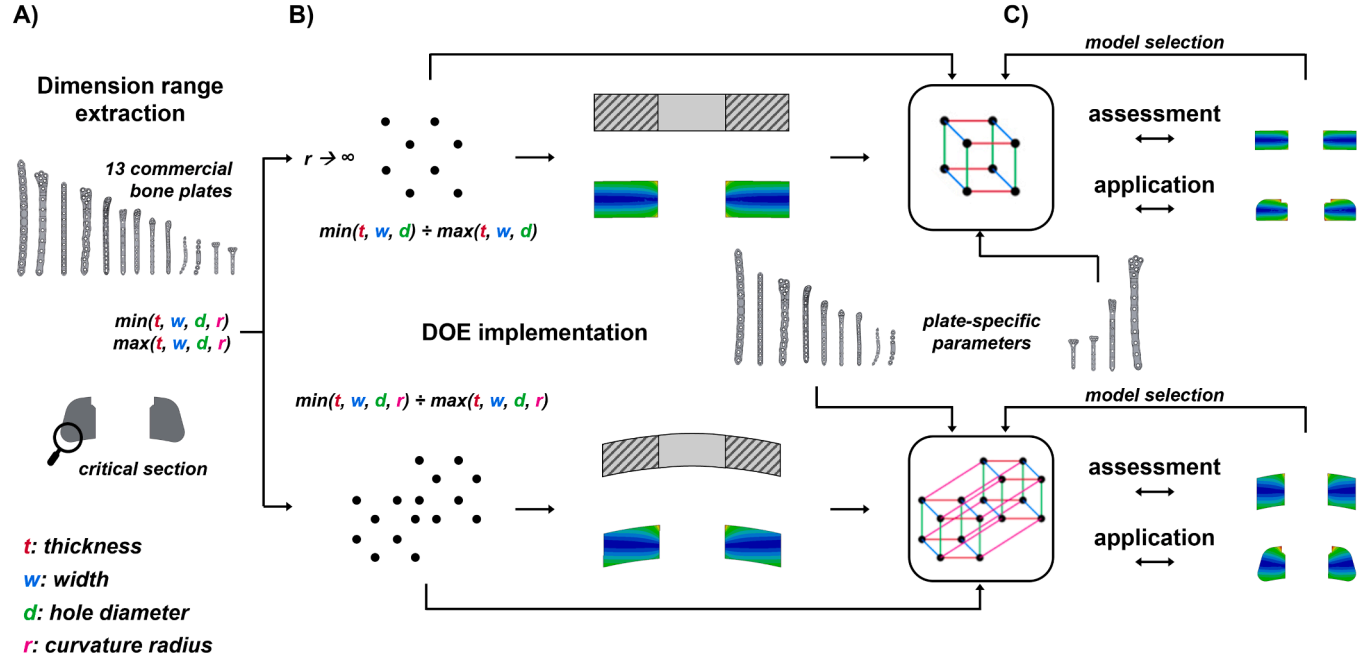


Fig. 1. Workflow of the proposed framework. A) Extraction of the geometric parameters from thirteen commercial bone plates. B) Development of SP models through DOE and FE simulations for flat and cross-curved plates. C) Assessment and application of the SP models for SCF estimation in simplified plate geometries and geometrically faithful 3D commercial bone plates.

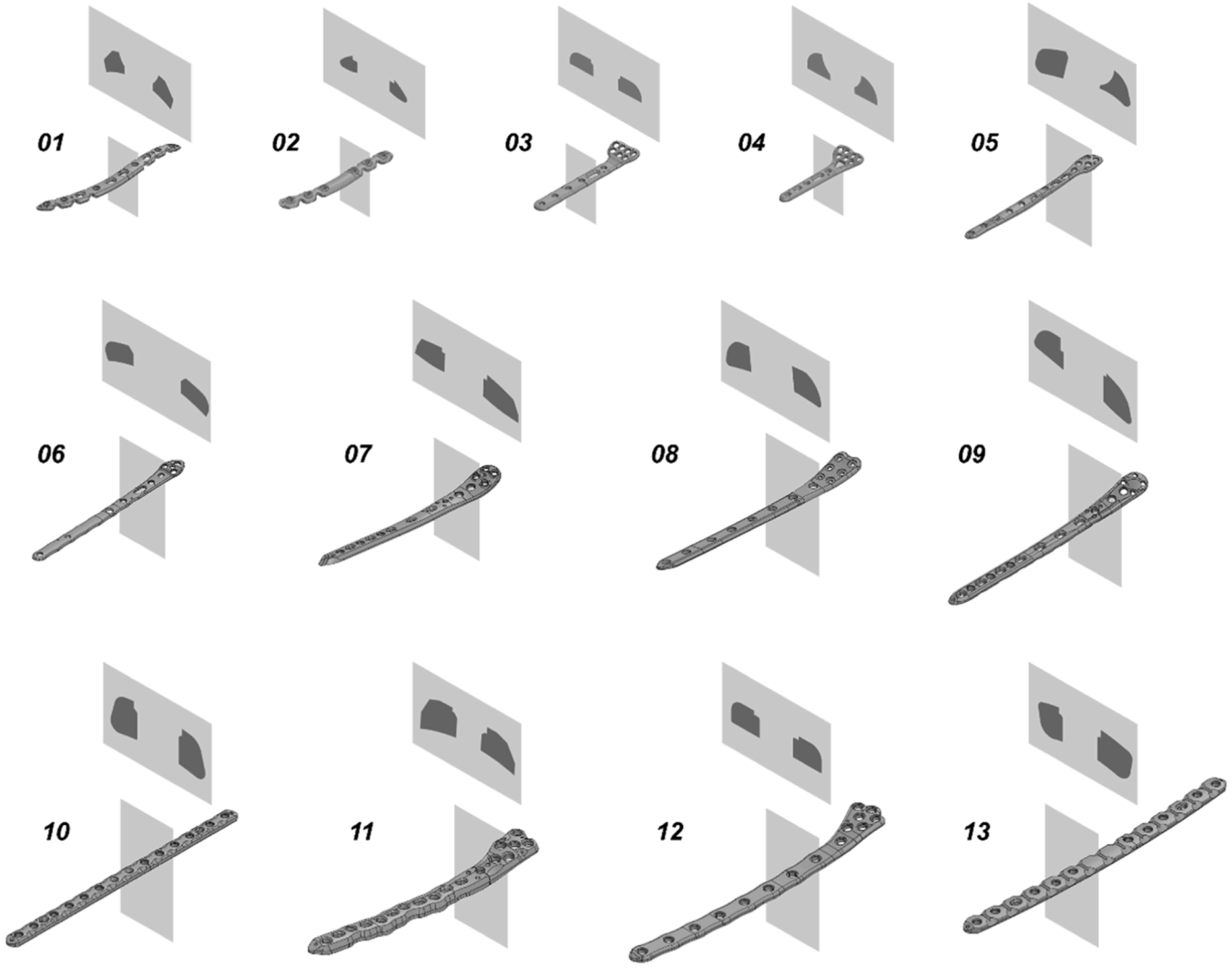


Fig. 2. Thirteen commercial bone plates used for the extraction of geometric parameters at their critical cross-section. The dimensions of the plates are shown to scale.

commercially available plates [19], to encompass plates designed for the following anatomical regions: wrist, malleolus, clavicle, tibia (distal and diaphyseal), and femur (distal and diaphyseal). For each plate geometry, an *ad hoc* function [4] developed in MATLAB R2020b (MathWorks, Natick, MA, USA) was used to automate the extrapolation of the thickness (t), width (w), and diameter (d) in the cross-section of the bone plate with the lowest moment of inertia (J). The hole diameter (d) was set equal to the internal diameter of the hole, excluding any countersinks or undercuts designed to accommodate screw heads, which are typically not present in early-stage design. A smaller diameter is also more conservative in terms of SCF estimation. Instead, the curvature radius (r) at the extrados of the critical section was manually extracted using SolidWorks 2020 (Dassault Systèmes, Vélizy-Villacoublay, France). Specifically, the value was obtained by interpolating a circle through four manually selected points along the extrados curvature profile. Both the internal and external radii of curvature were set to be equal to the extrados curvature radius.

The minimum, maximum, and median values for the key dimensions of the selected plates, including the ratios between hole diameter and thickness (d/t) and diameter to width (d/w) are listed in Table 1. All extracted values are provided in the supplementary section (Table S1).

Table 1
Minimum, maximum, and median dimension of selected bone plates.

	Minimum	Maximum	Median
t (mm)	1.5	5.2	3.0
w (mm)	8.9	18.9	12.5
d (mm)	3.1	6.5	5.5
r (mm)	9.7	500.0	56.3
d/t	1.02	3.21	1.59
d/w	0.16	0.73	0.38

DOE implementation

The parameter ranges were defined using the extreme values (minimum and maximum) of the commercial bone plates, excluding intermediate dimensions (Table 1). These geometric parameters were then used as inputs for a full factorial DOE [20] with six levels per parameter, covering all possible combinations, resulting in a total of 1296 configurations. These combinations were then used as inputs for a simplified parametric FE model developed in Ansys Workbench 2020 R2 (Ansys Inc., Canonsburg, PA, USA) to perform the virtual DOE, as shown in Fig. 3 (left). A perpendicular force of 10 N was applied to one side of the plate, while the opposite side was constrained (Fig. 3, right). This loading condition was adopted to determine the stress concentration

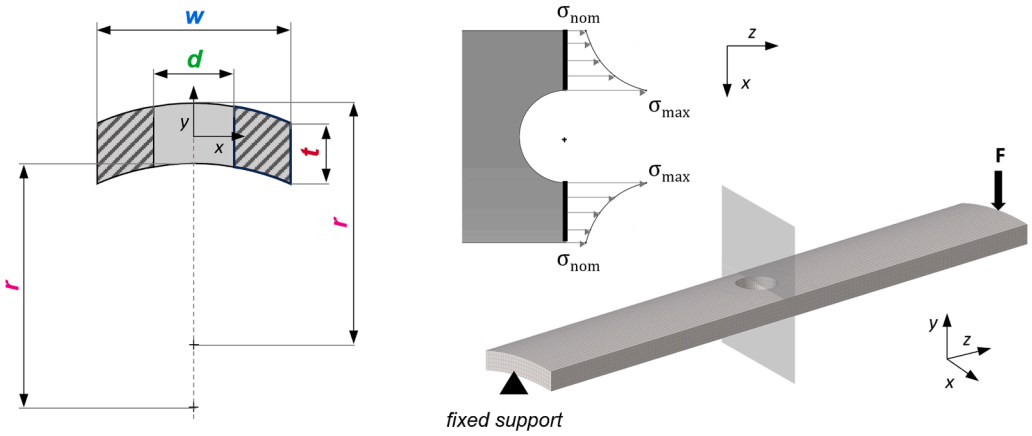


Fig. 3. Parametric FE model. (Left) Geometric parameters implemented in the FE model and cross-sectional view at the hole location. (Right) Boundary conditions applied to the parametric model, with a bending force *(F)* and fixed constraint. The local stress amplification near the hole is qualitatively represented.

factor under an idealised pure bending condition representative of the constant-moment region of ASTM F382-24 four-point bending, rather than of the complete test configuration. All the simplified plates were meshed with a 20-node 3D structural hexahedron second-order solid element (SOLID186). The mesh size was 0.3 mm for the central part of the plate where the hole feature is present, and 0.5 mm for the remaining plate geometry (See Supplementary Fig. S1, mesh convergence analysis for simplified plates).

The simplified parametric FE model was defined based on the geometry of the critical section, which was extruded along the longitudinal axis to create a simplified curved bone plate with a constant length of 100 mm. All FE simulations were performed on twelve computing cores of a workstation equipped with Intel® Core™ i7–12,700 and 32 GB RAM.

Importantly, the specific parameter combinations of the commercial bone plates were not directly included in the DOE simulations but were retained for the subsequent validation of the surrogate polynomial model.

To avoid unrealistic geometries, the curvature radius was capped at a maximum of 112.0 mm. This value corresponds to the condition where the sagitta (i.e., the maximum distance between a chord and the corresponding arc) equals 1% of the minimum plate width found among the commercial samples. Additional details on this threshold and its derivation are provided in Appendix B. For curvature radii greater than 112.0 mm, the plates were considered effectively flat, and the radius was excluded as a design parameter. This choice allowed for a more focused investigation of the influence of smaller curvature radii. In addition, a dedicated sub-DOE with three parameters (*t, w, d*) was generated for flat plates, resulting in a total of 216 configurations.

The nominal (σ_{nom}) and maximum (σ_{max}) stresses were computed: σ_{max} is maximum stress occurring at the edge of the hole (Fig. 3), and σ_{nom} is the nominal stress far from the discontinuity. In the case of simple bending, the nominal stress is calculated using the following equation:

$$\sigma_{nom} = \frac{My}{J} \tag{1}$$

where M is the bending moment, J is the moment of inertia of the cross-section about the neutral axis, and

y is the distance from the neutral axis.

Consequently, the SCF was calculated for all 1296 cases using Eq. (2), by dividing the maximum stress at the hole obtained from the FE analysis by the nominal stress computed using Eq. (1).

$$SCF = \frac{\sigma_{max}}{\sigma_{nom}} \tag{2}$$

Finally, the MATLAB function '*polyfitn*' [21] was used to derive the surrogate polynomial (SP) model based on the FE results, using first-, second-, and third-order polynomial fits. The third-order model includes 35 coefficients (a_n), which were computed for the general polynomial form reported below:

$$\begin{aligned} SCF(t,w,d,r) = {} & a_0 + a_1 t + a_2 w + a_3 d + a_4 r + a_5 t^2 + a_6 tw + a_7 td + a_8 tr \\ & + a_9 w^2 + a_{10} wd + a_{11} wr + a_{12} d^2 + a_{13} dr + a_{14} r^2 + \ldots \\ & + a_{34} r^3 \end{aligned} \tag{3}$$

The accuracy of the SCF values predicted by the SP models was evaluated using a linear least squares (LLS) analysis. Deviations were quantified with respect to the 45° reference line, representing perfect agreement between predicted and simulated values ($R^2 = 1$). Model robustness was further assessed and confirmed using leave-one-out cross-validation (LOOCV), with detailed results reported in the Supplementary Material (Fig. S4). To further investigate the influence of the geometric parameters on the predicted SCF and to complement the global validation framework, sensitivity analyses were performed on the developed SP models (see Sensitivity Analysis section in the Supplementary Material). For both models, a global screening was first conducted using Partial Rank Correlation Coefficients (PRCC) to quantify the monotonic relationships between input parameters and SCF across the full design space. This was followed by a one-at-a-time (OAT) analysis, in which each parameter was varied independently over its design range while the remaining variables were fixed at their central values, in order to capture local trends in the surrogate response.

Regarding the cross-curved plate model, the specific role of curvature was examined in greater detail through a refined analysis in which the curvature radius was systematically varied under different combinations of the remaining geometric parameters, allowing interaction effects between curvature and the other variables to be explored. A comprehensive description of the methodology and the corresponding results are provided in the Supplementary Material (Figs. S5–S9).

SP model assessment

Combinations of geometric parameters extracted from thirteen commercially available bone plates were used to assess and select the most appropriate order of the SP model. The evaluation was carried out by running thirteen additional simulations, in which the simplified parametric FE model was used with input values corresponding to the specific geometric parameters at the critical sections of the commercial bone plates.

To improve prediction accuracy, flat plates were evaluated separately from those with cross-sectional curvature, allowing predictions to

remain within the respective simulated ranges. The parameters of the commercial plates were allocated to one of the two SP models based on the radius of curvature: nine plates with a curvature radius <112.0 mm were used to test the model for curved plates with a circular hole, while the remaining four sets of parameters were used to assess the model for flat plates with a circular hole.

As part of this assessment phase, a second LLS analysis was performed using these non-DOE geometric parameters to quantify the predictive performance of the SP models outside the original DOE space. This analysis provided additional insight into the robustness and generalizability of the surrogate models when applied to geometrically faithful 3D plate designs.

For practical application, the SCF calculation procedure was implemented in a standalone graphical user interface (GUI) developed in MATLAB [22]. Users are required to upload the bone plate geometry in STL format. Subsequently, the application automatically evaluates the moment of inertia (J) of the critical section and the SCF based on the SP model. In this section, the user manually selects four points along the extrados curvature profile for the curvature assessment. These points are then used to interpolate a circle for calculating the curvature radius.

SP model application

The maximum stress at the critical section of thirteen commercial bone plates was evaluated based on their faithful 3D geometries. In the first stage, a FE analysis was performed for each bone plate using simplified boundary conditions (Fig. 4). Specifically, one end of the plate was fully constrained, while a force of 10 N was applied to the opposite end to simulate a simplified bending condition.

For the mesh, the thirteen commercial bone plates were subdivided into three groups – large, medium, small – based on their length. From each group, a bone plate was selected to perform the mesh convergence analysis [23,24]. A 10-node tetrahedral second-order structural solid element (SOLID187) was chosen due to the irregular shape of the plates. For the large group, 0.70 mm mesh size was chosen; 0.25 mm for the medium group of plates, and 0.20 mm for the small group of bone plates (See Supplementary Figs. S2-S3, mesh convergence analysis for geometrically faithful 3D plates).

The corresponding maximum stress value at the critical section was subsequently extracted for each bone plate.

In the second stage, the STL geometry of each plate was uploaded to the GUI to automatically compute the SCF and the moment of inertia (J), which are used to analytically determine the maximum stress through Eqs. (1) and 2.

Finally, the performance of the SP model was evaluated by quantifying the error between the maximum stress derived from the FE model and that obtained from the GUI.

Results

SP model for flat plates with a circular hole

All SP models achieved coefficients of determination (R^2) greater than 0.98 during the training phase; however, the first-order model was selected due to its superior performance in the assessment phase (R^2 = 0.91). The response surfaces generated from the first-order model (Fig. 5) show good agreement with the corresponding FE simulations (see Supplementary Fig. S10), particularly in the region where $d/w >$ 0.30, with all percentage errors remaining below 5%.

As expected, higher SCFs were associated with configurations featuring smaller holes and thicker plates. The parameter space was defined to include a minimum d/t ratio of 0.60, intentionally below the typical threshold for thin plates. The highest SCF value (1.86) occurred in a configuration with $t = 5.2$ mm, $w = 18.9$ mm, and $d = 3.1$ mm (d/w = 0.16, $d/t = 0.60$), while the lowest value (1.16) was observed for t = 1.5 mm, w = 8.9 mm, and d = 6.5 mm (d/w = 0.73, d/t = 4.33). A general trend of decreasing SCF with increasing d/w and decreasing t was noted. Interestingly, for d/w ratios exceeding 0.30, particularly in configurations with large hole diameters and small widths, this trend reversed, resulting in a sudden increase in SCF.

SP model for cross-curved plates with a circular hole

The second-order polynomial model was selected for cross-curved plates (r < 112.0 mm), showing the best assessment performance (R^2 = 0.95) and minimal drop from training. The first-order model resulted in a lower predictive capability (R^2 = 0.84), suggesting that the linear formulation was not sufficient to capture the nonlinear influence of cross-curvature on SCF. The third-order model provided comparable but not superior performance, indicating that additional polynomial terms did not significantly improve the model accuracy.

The surfaces of the second-order SP model for the parameter sets employed in constructing the DOE were plotted to visualise their behaviour and the difference from the simulated SCF values (Fig. 6). The surfaces of the SP model with r = 9.7 mm show the largest variations compared to the simulated points plates (See Supplementary Fig. S11). Specifically, the largest negative percentage error (around 9%) occurs at the point with $t = 1.5$ mm, $w = 8.9$ mm, and $d = 6.5$ mm ($d/w = 0.73$, d/t = 4.33), while the largest positive percentage error (around 8%) occurs at the point with $t = 1.5$ mm, $w = 18.9$ mm, and $d = 3.1$ mm ($d/w = 0.16$, $d/t = 2.07$).

Consistent with the DOE simulations for flat plates, the maximum SCF value was observed for the configuration with $t = 5.2$ mm, $w = 18.9$ mm, and $d = 3.1$ mm ($d/w = 0.16$, $d/t = 0.60$). The introduction of cross curvature led to a variation in the SCF. Indeed, in the case with

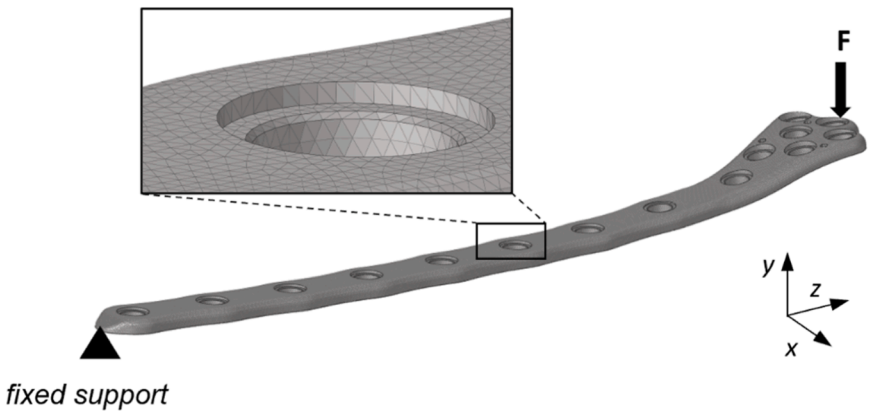


Fig. 4. FE model showing the boundary conditions applied to a representative commercial bone plate, with a perpendicular force (F) and fixed constraint. Top left: magnified view of the mesh at the hole region, defined as the critical cross-section.

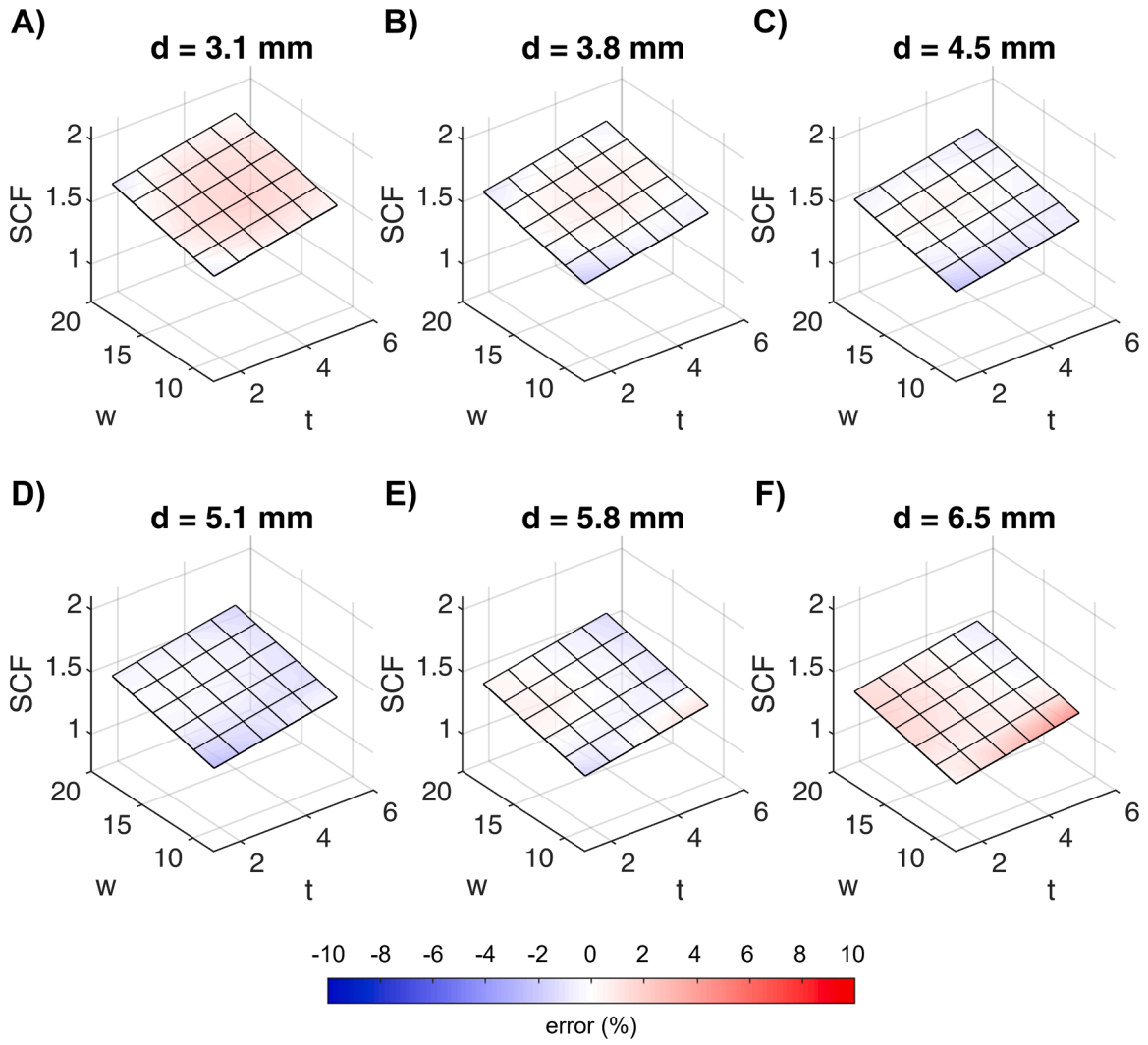


Fig. 5. Response surfaces of first-order SP model as a function of width and thickness with increasing hole diameters for $d = 3.1$ mm (A), $d = 3.8$ mm (B), $d = 4.5$ mm (C), $d = 5.1$ mm (D), $d = 5.8$ mm (E), and $d = 6.5$ mm (E). The color scale indicates the error (%) for each point in the SP model compared to the simulated SCFs.

maximum cross curvature ($r = 9.7$ mm), an increase of almost 5% (SCF = 1.95) was observed with respect to the flat plate. In the same configuration with the minimal cross curvature ($r = 112.0$ mm) a value of SCF = 1.84 was observed, indicating a minimal variation of approximately 1%, confirming the similarity to the flat plate.

Even the lowest value of the SCF remained consistent with the simulations of the flat plate, identified for the configuration with $t = 1.5$ mm, $w = 8.9$ mm, and $d = 6.5$ mm ($d/w = 0.73$, $d/t = 4.33$). In this limiting case with $d/w > 0.3$, the influence of cross curvature resulted in a decrease in the SCF. In the case with $r = 112.0$ mm, the reduction was approximately 6% (SCF = 1.09). However, in the case with $r = 9.7$ mm, the reduction was as high as 31% (SCF = 0.80), corresponding to the point with the greatest reduction induced by cross curvature. Conversely, the configuration that exhibited an increase in the SCF was that with $t = 1.5$ mm, $w = 18.9$ mm, and d = 3.1 mm ($d/w = 0.16$, $d/t = 2.07$). In this case, an increase of 18% was observed (SCF = 1.95) compared to simulations on a flat plate.

SP model application

The coefficients of the selected SP models (Eq. (3)), first-order for flat plates and second-order for cross-curved plates, are summarized in Table 2. For the second-order cross-curved models, coefficients associated with terms exhibiting p-values greater than 0.05 were set to zero, ensuring a parsimonious formulation and reducing the risk of overfitting.

To validate the practical application of the models, the SCFs estimated using the SP models were compared with those obtained from FE analysis for thirteen commercial bone plates.

Fig. 7 presents the absolute percentage error for each plate. The results highlight a generally strong agreement between the SP models and FE simulations. The lowest error (0.5%) was observed for *Plate08 and Plate13*, while *Plate04* and *Plate05* showed the highest errors, reaching 14.4% and 15.1%, respectively. Notably, all error values remained below the 16% threshold. Specifically, five plates exhibited errors below 5%, six were between 5% and 10%, one was between 10% and 15%, and only one plate slightly exceeded 15%. These findings support the reliability of the proposed SP models for rapid SCF estimation in real-world implant geometries, while significantly reducing computational time compared to full FE simulations.

FE results for all critical cross-sections are provided in Supplementary Fig. S12.

Discussion

The surrogate-based approach proposed in this study enables fast and geometry-based estimation of peak bending stress in bone plates with circular holes, handling both flat and cross-curved geometries. Its

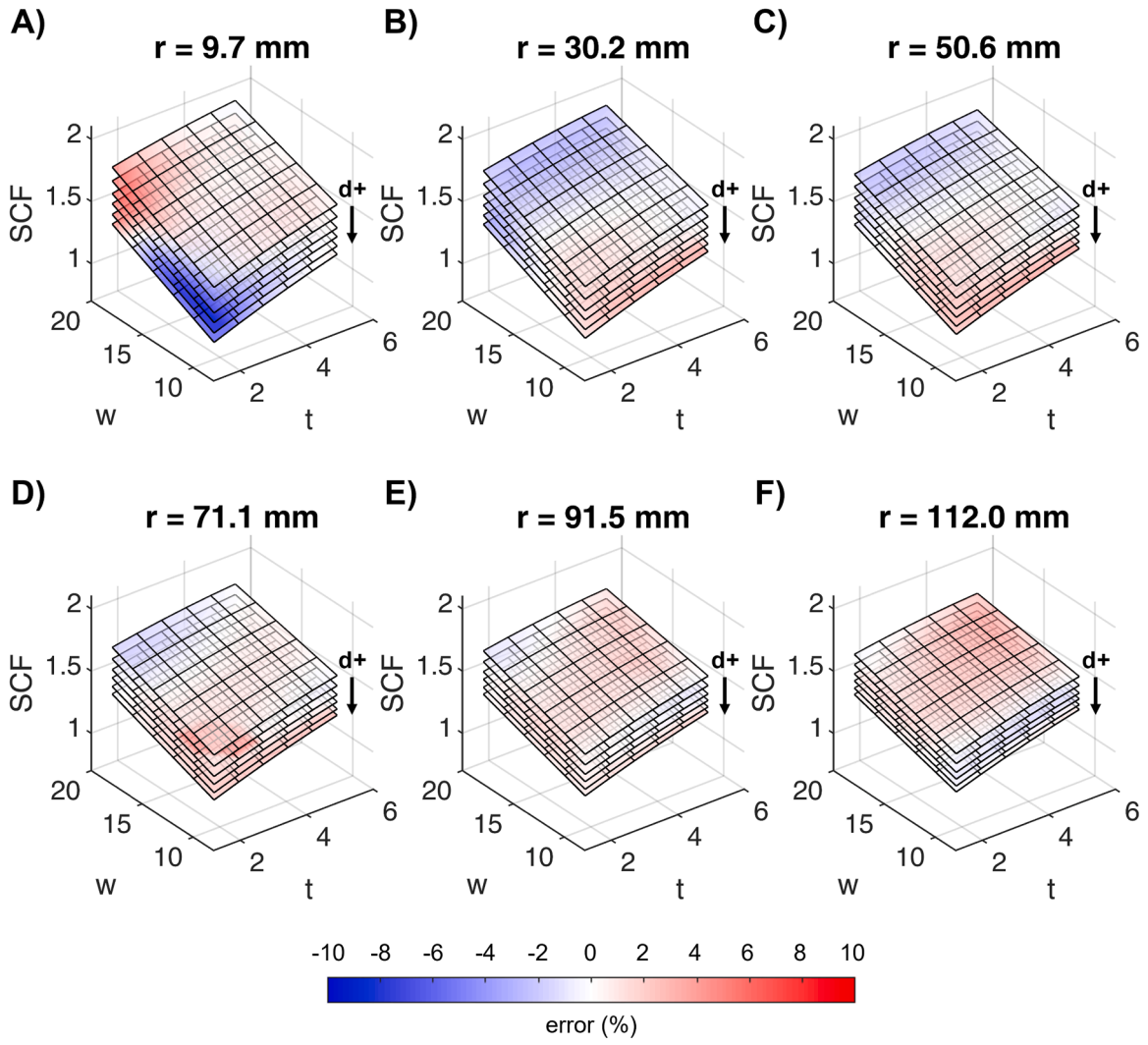


Fig. 6. Response surfaces of second-order SP model as a function of width and thickness with increasing hole diameters (black arrow) for $r = 9.7$ mm (A), $r = 30.2$ mm (B), $r = 50.6$ mm (C), $r = 71.1$ mm (D), $r = 91.5$ mm (E), and $r = 112.0$ mm (F). The color scale indicates the error (%) for each point in the SP model compared to the simulated SCFs.

Table 2
Coefficients of the SP models for flat and cross-curved plates.

	Flat plates	Cross-curved plates
a_0	1.480E+00	1.361E+00
a_1	5.107E-02 mm^{-1}	1.267E-01 mm^{-1}
a_2	2.077E-02 mm^{-1}	5.144E-02 mm^{-1}
a_3	−8.938E-02 mm^{-1}	−2.161E-01 mm^{-1}
a_4	-	6.792E-04 mm^{-1}
a_5	-	−4.043E-03 mm^{-2}
a_6	-	−3.518E-03 mm^{-2}
a_7	-	3.332E-03 mm^{-2}
a_8	-	−1.204E-04 mm^{-2}
a_9	-	-
a_{10}	-	−4.363E-04 mm^{-2}
a_{11}	-	−1.631E-04 mm^{-2}
a_{12}	-	8.450E-03 mm^{-2}
a_{13}	-	3.897E-04 mm^{-2}
a_{14}	-	-

primary utility lies in the early-stage implant design process, where quick evaluations of mechanical performance are essential to guide geometry selection and refinement. Traditional approaches at this stage often rely on engineering handbooks or lumped-parameter models tailored to simple geometries. However, these tools are not directly

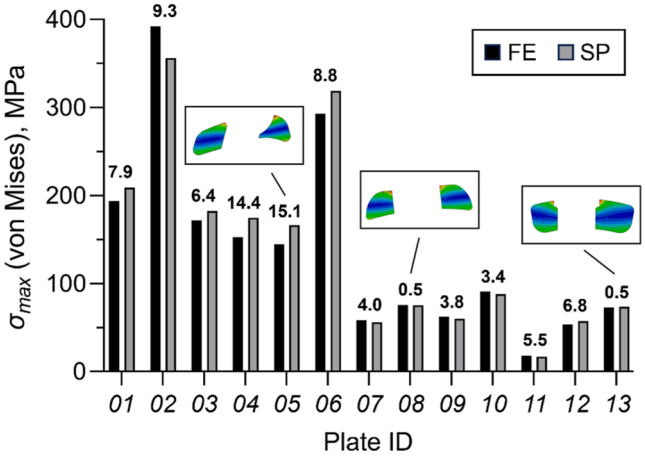


Fig. 7. Comparison of maximum stress in the critical section of thirteen commercial bone plates as predicted by the SP and FE models. The percentage error between the two methods is shown above each bar pair. Insets display the critical sections of the plate with the smallest error (*Plate08* and *Plate13*) and the plate with the largest error (*Plate05*), respectively.

applicable to bone plates due to their complex shapes and anatomical curvatures.

To bridge this gap, a comprehensive DOE was developed to extend theoretical formulations for SCF estimation, incorporating the main geometric features of commercial bone plates, including the effect of cross curvature.

To facilitate practical application, an open-access MATLAB GUI [22] was developed to compute SCF values based on the geometry of the plate. The critical cross-section is automatically identified, its moment of inertia is calculated, and the SCF is estimated using SP models trained on FE simulations. This approach aims to accelerate the assessment of multiple design variants prior to committing to full FE simulations and is particularly valuable when licensing restrictions, time constraints, or the need for extensive design iterations render FE analyses impractical.

Two SP models were developed to estimate the SCF, using a curvature radius threshold of 112.0 mm to differentiate the models. For both flat plates and those with curvature radius $r > 112.0$ mm, a third-order polynomial model better fitted the training data. However, during testing, the first-order polynomial model outperformed the third-order one for flat plates, indicating a potential overfitting in the training phase. For plates with $r \leq 112.0$ mm (i.e., plates with cross curvature), the training data more closely, the second-order polynomial model showed superior predictive performance on testing data. Hence, the second-order model was selected for cross-curved plates due to its more balanced accuracy between training and testing phases.

A significant variation in results between the model for flat plates and the one with cross curvature is present for small curvature radii, confirming the importance of considering the curvature effect for SCF calculation. In fact, at the point of maximum difference between the two SP models, the difference in SCF calculation reaches up to 18%. To the author's knowledge, such consideration has only been made for longitudinally curved beams, where an increase of 10% in stresses is typically reported if the mean radius of curvature ($\bar{r}$) is at least 10 times greater than the distance between the surface and the neutral axis (y_{max}) [25].

Finally, an assessment of the performance of the SP models in evaluating the maximum stress on the critical section of bone plates was conducted. For most plates (eleven out of thirteen), the strong agreement between the SP and FE models indicates that, for these configurations, the SP models effectively capture the maximum stress in the critical sections of the plates, with accuracy closely matching that of the model. This result highlights the potential of the SP models as a practical tool in preliminary design evaluations.

However, two out of thirteen plates (*Plate04* and *Plate05*) showed significant deviations from the general trend. These inconsistencies may arise from the complex cross-sectional morphology of the geometrically faithful 3D bone plates, particularly the shape of the section and the moment of inertia, which can influence stress estimation accuracy. In both cases, the plates featured hemispherical recesses for compression screws.

This study also presents some limitations. Firstly, the curvature radius is the only parameter that has not been automatically extracted. This decision was made due to the different cross curvatures present in commercial plates, which cannot be easily simplified with a single interpolating circumference. For this reason, it was decided to extract this parameter through user input. Additionally, to maintain constant plate thickness, the curvature radius of the intrados was set equal to that of the extrados. The extrados region is indeed the most critical for a bending test, but the effect of a different curvature in the intrados was neglected. This aspect could potentially influence cases involving plates with an almost flat extrados and cross curvature on the intrados side, which might be beneficial, for instance, in conforming to the profile of a healing bone. Moreover, except for more tapered lateral regions, the thickness of the examined commercial plates was assumed to be practically constant. A similar assumption was made for the hole diameter: by treating the hole as perfectly cylindrical, additional stress concentrations associated with screw head seating features, such as spherical recesses used in compression screws, were not considered. The loading condition considered throughout the study was not intended to reproduce either physiological in vivo loading or the ASTM F382-24 experimental configuration. Rather, it represents an idealised pure bending condition adopted to isolate the geometry-dependent stress concentration factor. The resulting SCFs can subsequently be combined with the nominal bending stress associated with a given loading scenario, including the constant-moment region of the ASTM four-point bending test, although the present study does not simulate the complete experimental setup.

Despite these limitations, the SP models developed in this study allow for rapid SCF estimation for both flat and cross-curved plates without the need for dedicated FE simulations. Compared to FE analyses, which require time for model setup, meshing, and post-processing, the proposed approach provides immediate and easily accessible evaluation of the peak bending stress.

Conclusion

This study has developed and validated DOE strategies to extend existing theoretical formulations for the calculation of SCFs in bone plates. New SP models were derived to accurately predict SCFs for flat plates with diameter-to-width ratios exceeding 0.30, a range relevant to commercial bone plates. Additionally, a novel polynomial formulation was introduced to capture the effect of cross curvature on SCFs, addressing a key geometric feature of anatomically contoured bone plates that has been largely neglected in previous analytical methods.

The proposed computational approach enables fast and reliable estimation of peak bending stresses in bone plates with circular holes without requiring full FE analyses. It is particularly relevant for standardised mechanical testing, such as the ASTM F382 four-point bending configuration, where rapid stress evaluation can support test planning and interpretation. This capability is especially valuable during early-stage implant design, facilitating rapid exploration and optimization of complex plate geometries incorporating cross curvature. Ultimately, these findings contribute to improved biomechanical assessment and design of anatomically shaped bone plates by bridging the gap between simplified analytical models and computationally intensive numerical simulations.

CRediT authorship contribution statement

Federico Andrea Bologna: Writing – original draft, Visualization, Investigation, Conceptualization. **Ulyana Konopada:** Validation, Software, Data curation. **Dario Carbonaro:** Writing – review & editing, Methodology. **Alberto Audenino:** Supervision, Resources. **Mara Terzini:** Writing – review & editing, Supervision.

Declaration of competing interest

The authors declare that they have no known competing financial interests or personal relationships that could have appeared to influence the work reported in this paper.

Supplementary materials

Supplementary material associated with this article can be found, in the online version, at doi:10.1016/j.rineng.2026.111990.

Appendix A

The formulas below were used in the main text for comparison purposes. They represent the analytical expressions by Roark as detailed by Young and Budynas [12], for infinite and finite-width plates under transverse bending.

Infinite thin plates

For infinite plates subjected to transverse bending, the stress concentration factor K_{tn}^{∞} is given by:

$$K_{tn}^{\infty} = 1.79 + \frac{0.25}{0.39 + (d/t)} + \frac{0.81}{1.00 + (d/t)^2} - \frac{0.26}{1.00 + (d/t)^3} \tag{A.1}$$

for $\nu = 0.3$ and $0 \leq d/t \leq 7.00$.

Finite-width plates

For finite-width plates subjected to transverse bending, Roark's analytical formulation is:

$$K_{tn} = \left[1.79 + \frac{0.25}{0.39 + (d/t)} + \frac{0.81}{1.00 + (d/t)^2} - \frac{0.26}{1.00 + (d/t)^3}\right] \cdot \left[1.00 + 1.04\left(\frac{d}{w}\right) + 1.22\left(\frac{d}{w}\right)^2\right] \tag{A.2}$$

for $\nu = 0.3$, $1.0 \leq d/t \leq 7.00$, and $0 \leq d/w \leq 0.30$, where K_{tn} is the SCF in finite-width plates.

Young and Budynas [12] state that for most of the specified variable ranges, these curves fit the experimental data with <5% error.

Appendix B

The curvature radius was capped at a maximum of 112.0 mm. This value was determined by imposing that the sagitta (h), defined as the vertical distance between a chord and the corresponding arc (see Fig. B1), equals 1% of the minimum plate width among the commercial samples ($w_{min} = 8.93$ mm).

The sagitta is computed from the curvature radius (r) and chord length (w) using the following geometric relation:

$$h = r - \sqrt{r^2 - \left(\frac{w}{2}\right)^2} \tag{B.1}$$

where w represents the plate width.

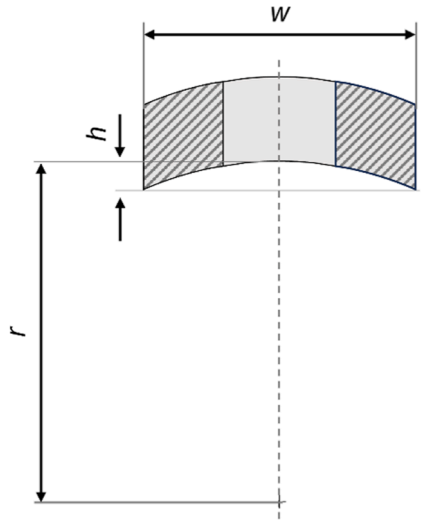


Fig. B1. Cross-sectional view at the hole location, showing the geometric relationship between the curvature radius (r), chord length (w), and sagitta (h).

Data availability

Data will be made available on request.

References

[1] F. Burny, M. Donkerwolcke, F. Moulart, R. Bourgois, R. Puers, K. Van Schuylenbergh, et al., Concept, design and fabrication of smart orthopedic implants, Med. Eng. Phys. 22 (2000) 469–479, https://doi.org/10.1016/S1350-4533(00)00062-X.

[2] C. Sommer, E. Gautier, M. Müller, D.L. Helfet, M. Wagner, First clinical results of the locking compression plate (LCP), Injury 34 (2003) 43–54, https://doi.org/10.1016/j.injury.2003.09.024.

[3] ASTM International. Standard specification and test method for metallic bone plates F382-24, West Conshohocken, USA, 2024, https://doi.org/10.1520/F0382-24.

[4] F.A. Bologna, A.L. Audenino, M. Terzini, Bone plates runout prediction through tensile strength and geometric properties for regulatory mechanical testing, Ann. Biomed. Eng. 52 (2024) 239–249, https://doi.org/10.1007/s10439-023-03363-2.

[5] B. Muthusamy, C.K. Chao, S.J. Su, C.W. Cheng, J. Lin, Effects of merged holes, partial thread removal, and offset holes on fatigue strengths of titanium locking plates, Clin. Biomech. 96 (2022) 105663, https://doi.org/10.1016/j.clinbiomech.2022.105663.

[6] V. Wagare, R. Hundekari, Fatigue life and damage prediction of plate with central hole using finite element method, J. Mater. Sci. Surf. Eng. Fatigue 3 (2015) 202–206.
[7] D. Mischler, M. Glyde, M. Kowaleski, A. Vautrin, S. Lambert, P. Varga, Influence of plate working length on fatigue life in load bearing osteosynthesis constructs: Experimental insights and validated finite element predictions, J. Mech. Behav. Biomed. Mater. 175 (2026) 107322, https://doi.org/10.1016/j.jmbbm.2025.107322.
[8] W.J. Tseng, C.K. Chao, C.C. Wang, J. Lin, Notch sensitivity jeopardizes titanium locking plate fatigue strength, Injury 47 (2016) 2726–2732, https://doi.org/10.1016/j.injury.2016.09.036.
[9] M. Terzini, A. Aldieri, S. Nurisso, G. De Nisco, C. Bignardi, Finite element modeling application in forensic practice: a periprosthetic femoral fracture case study, Front. Bioeng. Biotechnol. 8 (2020) 1–11, https://doi.org/10.3389/fbioe.2020.00619.
[10] P.P. Kenedi, L.L. Vignoli, An osteosynthesis plate analytical model, J. Brazilian Soc. Mech. Sci. Eng. 39 (2017) 645–659, https://doi.org/10.1007/s40430-016-0598-3.
[11] W.D. Pilkey, Peterson's Stress Concentration Factors, 2nd ed., Wiley, New York, USA, 2008 https://doi.org/10.1002/9780470211106.ch3.
[12] W.C. Young, R.G. Budynas, Roark's formulas for stress and strain, 7th Ed., ed., McGraw-Hill, New York, USA, 2002 https://doi.org/10.1016/B978-0-444-41899-9.50020-3.
[13] Z. Yang, C.-B. Kim, H. Gyu Beom, C. Cho, The stress and strain concentrations of out-of-plane bending plate containing a circular hole, Int. J. Mech. Sci. 52 (2010) 836–846, https://doi.org/10.1016/j.ijmecsci.2010.02.001.
[14] C. She, W. Guo, Three-dimensional stress concentrations at elliptic holes in elastic isotropic plates subjected to tensile stress, Int. J. Fatigue 29 (2007) 330–335, https://doi.org/10.1016/j.ijfatigue.2006.03.012.
[15] K. Bakhshandeh, I. Rajabi, F. Rahimi, Investigation of stress concentration factor for finite-width orthotropic rectangular plates with a circular opening using three-dimensional finite element model, Stroj. Vestnik/J. Mech. Eng. 54 (2008) 140–147.
[16] H. Nassiraei, Probabilistic modeling of degree of bending in FRP-strengthened offshore tubular X-joints, Sci. Rep. 15 (2025) 1–15, https://doi.org/10.1038/s41598-025-23024-9.1.
[17] E. Zavvar, S. Ehlers, P. Santos, Maximum stress concentration factors in DKT joints subjected to combined compression and tension loads, Ships Offshore Struct. (2025) 1–12, https://doi.org/10.1080/17445302.2025.2453668.
[18] E. Zavvar, F. Sousa, F. Taveira-pinto, P.R. Santos, Multivariate data analysis of maximum stress concentration factors in FRP-retrofitted two-planar KT-joints under axial loads for offshore renewables, J. Mar. Sci. Eng. 12 (2024) 1451, https://doi.org/10.3390/jmse12081451.
[19] R. Zdero, K. Gide, P. Brzozowski, E.H. Schemitsch, Z.S. Bagheri, Biomechanical design optimization of distal femur locked plates: a review, Proc. Inst. Mech. Eng. Part H, J. Eng. Med. 237 (2023) 791–805, https://doi.org/10.1177/09544119231181487.
[20] N.R. Draper, D.K.J. Lin, Response surface designs, in: S. Ghosh, C.R. Rao (Eds.), Handbook of Statistics 13, 1996, pp. 343–375.
[21] D'Errico, J. (2024). Polyfitn. Available at: https://www.mathworks.com/matlabcentral/fileexchange/34765-polyfitn Accessed February 23, 2024.
[22] U. Konopada, F.A. Bologna, D. Carbonaro, A. Audenino, M. Terzini, SCFOrtho – A MATLAB GUI for fast estimation of stress concentration factors in bone plates (Version 1.0), Zenodo (2025), https://doi.org/10.5281/zenodo.16384608.
[23] F.A. Bologna, N. Elena, D. Bentivoglio, A. Aprato, M. Terzini, C. Bignardi, et al., In Silico evaluation of the primary stability of acetabular revision cups: standard versus locking screws, J. Biomech. Eng. 147 (2025) 1–8, https://doi.org/10.1115/1.4068226.
[24] F.A. Bologna, G. Putame, A.L. Audenino, M. Terzini, Understanding the role of head size and neck length in micromotion generation at the taper junction in total hip arthroplasty, Sci. Rep. 14 (2024) 1–12, https://doi.org/10.1038/s41598-024-57017-x.
[25] R.C. Junivall, K.M. Marshek, Fundamentals of machine component design, 6th ed., Wiley, New York, USA, 2017.